

Reproducing kernel based evaluation of incompatibility tensor in field theory of plasticity

Y. Aoyagi

Department of Mechanical Engineering, Keio University, 3-14-1, Hiyoshi Kohoku-Ku, Yokohama, 223-8522, Japan

T. Hasebe*

Department of Mechanical Engineering, Kobe University, 1-1, Rokkodai Nada, Kobe, 657-8501, Japan

P. C. Guan and J. S. Chen

Civil & Environmental Engineering Department, UCLA, 5731 Bolter Hall, Los Angeles, CA 90095, USA

(Received March 25, 2008, Accepted November 24, 2008)

Abstract. This paper employs the reproducing kernel (RK) approximation for evaluation of field theory-based incompatibility tensor in a polycrystalline plasticity simulation. The modulation patterns, which is interpreted as mimicking geometrical-type dislocation substructures, are obtained based on the proposed method. Comparisons are made using FEM and RK based approximation methods among different support sizes and other evaluation conditions of the strain gradients. It is demonstrated that the evolution of the modulation patterns needs to be accurately calculated at each time step to yield a correct physical interpretation. The effect of the higher order strain derivative processing zone on the predicted modulation patterns is also discussed.

Keywords: incompatibility tensor; field theory; reproducing kernel approximation; dislocation substructure; crystal plasticity; finite element method.

1. Introduction

Dislocation substructures evolved during the course of plastic deformation can be roughly classified into two kinds, i.e., mechanically-necessary type and geometrically-necessary-type, although their distinctions have not been always made appropriately. Particularly, the evolution of the former, exemplified by the dislocation cells, has been confused with incidental of structures of tangled dislocations or even with subgrains, although it essentially stems from the collective behavior of tremendous number of interacting dislocations thus cannot be properly described by continuum mechanics-based approach. The developments of the latter, on the other hand, can in principle be

* Corresponding Author, E-mail: hasebe@mech.kobe-u.ac.jp

simulated based on continuum mechanics, but it requires incorporation of additional defect degrees of freedom responsible for dislocation rearrangements for effectively lowering the energy of the system. Historically, many attempts have been made in vein to reproduce the dislocation substructures either simply based on conventional settings of the crystal plasticity only with geometrically-necessary-type of dislocation density not taking into account of proper defect degrees of freedom.

An incompatibility tensor, given by the double curl of strain tensor in continuum mechanics, has recently been proposed for identification of deformation-induced, i.e., geometrically-necessary type, intra-granular substructures in metallic materials. For example, dense dislocation walls and microbands modeled by field theory based crystalline plasticity (Hasebe 2004a, 2004b, 2006, Aoyagi and Hasebe 2007). The accuracy of the incompatibility tensor-based substructure prediction, however, relies heavily on the numerical calculation of the higher-order differentiation. Standard C^0 -finite element approximation requires ad hoc averaging procedures in the higher order differentiation and thus induces considerable amount of errors.

This study introduces a reproducing kernel approximation (Liu *et al.* 1995, Chen *et al.* 1996) for the computation of incompatibility tensor. Reproducing kernel approximation offers flexibility in adjusting continuity, polynomial reproducibility, locality, and discretization adaptivity that are particularly effective for the proposed incompatibility tensor-based substructure identification. The method has been applied to application to a structural analysis in terms of gradient calculation (Wang *et al.* 2008). In this study, the effects of kernel function continuity, locality, and the order of basis functions in the reproduction kernel approximation on the predicted incompatibility tensor distribution are identified. Comparison of the results obtained by the standard finite element and the proposed reproducing kernel approximation is made in several numerical examples.

2. Incompatibility tensor

In the field theory of plasticity (Hasebe 2004a, 2004b, 2006, Aoyagi and Hasebe 2007), two tensors of the differential geometrical kinds, i.e., torsion tensor and curvature tensor, play crucial roles in describing not only dislocation and defect fields but also more generalized inhomogeneously deforming fields in any scale levels. The torsion and curvature tensors are defined respectively as,

$$S_{kl}^{\cdot j} = \Gamma_{[kl]}^j \quad (1)$$

$$R_{klm}^{\cdot \cdot \cdot n} = 2[\partial_{[k} \Gamma_{l]m}^n + \Gamma_{[k|p]}^n \Gamma_{l]m}^p] \quad (2)$$

where Γ_{kl}^j are the coefficients of connection expressing the relation between two adjacent frames, further given as a function of the metric tensor of the crystalline space, g_{ij} of g^{ij} i.e., $\Gamma_{ij}^k = (1/2)g^{kl}(\partial_j g_{li} + \partial_l g_{ij} - \partial_i g_{jl})$, while $[]$ represents the skew-symmetric part with respect to the indices enclosed in it. Here, the change in the metric tensor before and after deformation measures the strain. Particularly, the curvature tensor yields an additional physical interpretation (Hasebe 2004a) as a quantity which measures the degree of incompatible deformation (curvature of the Riemannian kind) driven out of compatibility (flat space of the Euclidean kind). For a crystalline space, the Einstein tensor of the curvature Eq. (2) corresponds to the so-called incompatibility tensor (2nd-order divergenceless tensor), i.e.,

$$\boldsymbol{\eta}_{ij} = R_{ij} + \frac{1}{2}g_{ij}R \tag{3}$$

where $R_{ij} \equiv R_{inj}^n$ is the Ricci curvature, and $R \equiv g^{ij}R_{ij}$ is called the scalar curvature. Note, the combination given in Eq. (3) satisfies the divergence free condition, i.e., $\nabla_j\{R_{ij} + (1/2)g_{ij}R\} = 0$. In the framework of continuum mechanics, the incompatibility tensor is further expressed as a double curl of plastic strain tensor, i.e.,

$$\boldsymbol{\eta}_{ij} = \epsilon_{ikl}\epsilon_{jmn}\partial_k\partial_m\boldsymbol{\epsilon}_{ln}^p \tag{4}$$

where ϵ_{ikl} is the permutation symbol.

Regarding the torsion tensor, since the closure failure of a crystalline space means the existence of dislocations, it physically accounts for dislocation density. The 2nd-rank dislocation density tensor α_{ij} is obtained by a contraction of the torsion tensor, and is further expressed as a curl of plastic distortion tensor β_{ij}^p , i.e.,

$$\alpha_{ij} = \frac{1}{2}\epsilon_{ikl}S_{kl}^{;j} = -\epsilon_{ikl}\partial_k\beta_{lj}^p \tag{5}$$

3. Constitutive equations

A constitutive equation applicable to BCC metals which relates slip rate $\dot{\gamma}^{(\alpha)}$ with effective stress $\tau^{*(\alpha)}$ has been proposed by Hasebe (2006) and Aoyagi and Hasebe (2007),

$$\dot{\gamma}^{(\alpha)} = \dot{A}_{SR}\tau_{disloc}^{*(\alpha)} \exp\left[\left|\tau_{disloc}^{*(\alpha)}\right| \cdot \exp B_{SR}\left(1 - \left|\frac{\tau_{disloc}^{*(\alpha)}}{K^{(\alpha)}}\right|^p\right)^q + C_{SR}\right]^{-1} \tag{6}$$

$$\tau_{disloc}^{*(\alpha)} = \langle \tau^{(\alpha)} - \tau_{Peierls}^{*(\alpha)} \rangle - \boldsymbol{\Omega}^{(\alpha)} \tag{7}$$

where $K^{(\alpha)}$ represents the drag stress responsible for isotropic hardening, $\boldsymbol{\Omega}^{(\alpha)}$ is the back stress contributing to kinematic hardening, $\dot{A}_{SR}, B_{SR}, C_{SR}$ are materials constants, and $\tau_{Peierls}^{*(\alpha)}$ represents the effective stress for overcoming the Peierls potential, i.e.,

$$\tau_{Peierls}^{*(\alpha)} = \hat{\tau}_{Peierls}^* \left[1 - \left\{\frac{kT}{\Delta G} \ln\left(\frac{\dot{a}}{\dot{\gamma}^{(\alpha)}}\right)\right\}^{1/q}\right]^{1/p} \tag{8}$$

Here $\hat{\tau}_{Peierls}^*$ is the threshold stress for $\tau_{Peierls}^{*(\alpha)}$ at absolute zero temperature, k the Boltzmann constant, T the temperature, ΔG the activation energy and \dot{a} the referential strain rate. The evolution of the drag stress $K^{(\alpha)}$ is given by,

$$\dot{K}^{(\alpha)} = Q_{\alpha\beta}H(\gamma)|\dot{\gamma}^{(\alpha)}| \tag{9}$$

where $Q_{\alpha\beta}$ denotes the hardening ratio, $H(\gamma)$ the hardening modulus, and $\gamma = \sum_{\alpha} \gamma^{(\alpha)}$ where $\gamma^{(\alpha)}$ is the slip strain in each slip system. In order to take into account the inhomogeneities in different scale levels, the dislocation density and incompatibility tensors are introduced as strain gradient

terms, $F(\alpha^{(\alpha)})$ and $F(\eta^{(\alpha)})$, into the hardening ratio i.e.,

$$Q_{\alpha\beta} = \delta_{\alpha\beta} + f_{\alpha\kappa} S_{\kappa\beta} + \delta_{\alpha\beta} F(\alpha^{(\alpha)}) + F(\eta^{(\alpha)}) \quad (\text{no sum on } \alpha) \quad (10)$$

where $f_{\alpha\kappa}$ is the dislocation interaction matrix and $S_{\kappa\beta}$ the matrix expressing the loading history further given as a function of plastic work in each slip system. From $Q_{\alpha\beta}$, the effective cell size is evaluated via

$$d_{cell} = k' \sqrt{Q_{\alpha\beta} Q_{\alpha\beta}} / N \quad (10')$$

where k corresponds to a fraction of the initial grain size and N is the number of slip systems.

The explicit forms of the strain gradient terms are proposed by Aoyagi and Hasebe (2007) as

$$F(\alpha^{(\alpha)}) = \frac{\bar{k}}{p_\alpha} \sqrt{\frac{|\alpha^{(\alpha)}|}{b}} \quad (11)$$

$$F(\eta^{(\alpha)}) = \text{sgn}(\eta^{(\alpha)}) \frac{\bar{k}}{p_\eta} \sqrt{\frac{l_{defect}}{b} |\eta^{(\alpha)}|} \quad (12)$$

where b denotes the magnitude of the Burgers vector and \bar{k} represents a referential size normally corresponding to the initial grain size, l_{defect} , p_α and p_η are the material constants, and $\alpha^{(\alpha)}$ and $\eta^{(\alpha)}$ are the resolved components of α_{ij} and η_{ij} into (α) slip system, respectively. In the present paper, the following projections are used,

$$\alpha^{(\alpha)} = s_i^{(\alpha)} m_j^{(\alpha)} \alpha_{ij} \quad (13)$$

$$\eta^{(\alpha)} = s_i^{(\alpha)} t_j^{(\alpha)} \eta_{ij} \quad (14)$$

where $s_i^{(\alpha)}$, $m_j^{(\alpha)}$ are unit vectors expressing the slip direction and slip plane normal, respectively, and $t_j^{(\beta)} = \epsilon_{ijk} s_j^{(\beta)} m_k^{(\beta)}$. Here the incompatibility tensor is resolved into slip line direction as indicated in Eq. (14) considering our purpose here, i.e., to mimic geometrical-type dislocation substructures based on a comparison with experimental observations (Sugiyama 2005).

4. Simulation model

Fig. 1 illustrates a multi-crystal model discretized into 96×96 C^0 -type crossed-triangle elements. Here, heterogeneity in the grain shapes, such as those numerically reproduced by Zhang *et al.* (2008) is ignored, assuming geometrically isotropic hexagonal shape. In the following, simulation results for displacements, strains and incompatibility tensors along the solid cross sectional line in grain 4 are shown. Intra-granular modulation formations on a similar model have been discussed in light of the geometrically-necessary type dislocation substructure evolutions (Aoyagi and Hasebe 2007). The model consists of seven grains of BCC iron accommodated with $\{110\}\langle 111 \rangle$ slip systems. Crystal orientations allocated to each grain are given in Fig. 1(b). Tension up to 20% nominal strain is applied to the FEM model. Plastic distortion field is evaluated based on the standard kinematics, i.e.,

$$\beta_{ij}^p = \sum_{\alpha} s_i^{(\alpha)} m_j^{(\alpha)} \gamma^{(\alpha)} \quad (15)$$

where $s_i^{(\alpha)}$, $m_j^{(\alpha)}$ are unit vectors expressing slip direction and slip plane normal, respectively. In

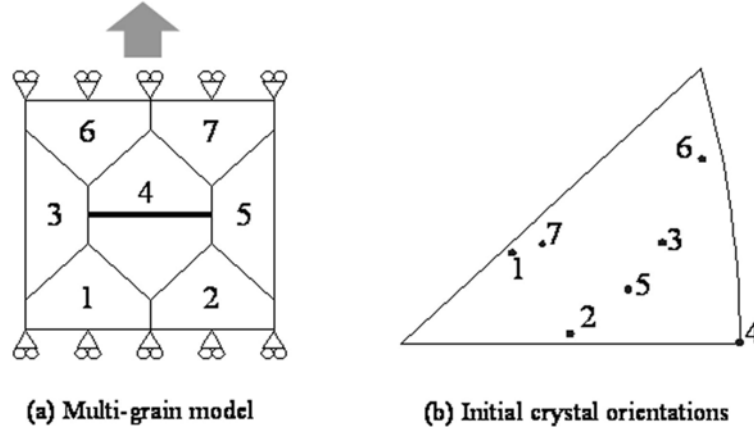


Fig. 1 Computational model

addition, total distortion is separately evaluated from the displacement field by utilizing the RK approximation, from which vanishing incompatibility tensor is further evaluated to confirm the accuracy of the method.

5. Reproducing kernel approximation

For an accurate evaluation of incompatibility tensor field via of Eq. (4) used in the strain gradient terms in Eqs. (10) and (11), we utilize the reproducing kernel approximation (Liu *et al.* 1995, Chen *et al.* 1996) in this work. The calculation of the incompatibility tensor needs approximation of displacement field with at least C^2 -continuity. The three-dimensional RK approximation is given by

$$\mathbf{u}^a(\mathbf{x}) = \sum_{I=1}^{NP} \bar{\Phi}^a(\mathbf{x}; \mathbf{x} - \mathbf{x}_I) \mathbf{u}_I \quad (16)$$

where \mathbf{u}^a is the RK approximation of \mathbf{u} , \mathbf{u}_I is the coefficient, a refers to the support size which will be explained later, NP is the number of discrete points, and, $\bar{\Phi}^a(\mathbf{x}; \mathbf{x} - \mathbf{x}_I)$, is the reproducing kernel expressed as,

$$\bar{\Phi}^a(\mathbf{x}; \mathbf{x} - \mathbf{x}_I) = \Phi^a(\mathbf{x} - \mathbf{x}_I) C(\mathbf{x}; \mathbf{x} - \mathbf{x}_I) \quad (17)$$

where $C(\mathbf{x}; \mathbf{x} - \mathbf{x}_I)$ is called the correction function used to impose polynomial reproducibility, and $\Phi^a(\mathbf{x} - \mathbf{x}_I)$ is the multi-dimensional kernel function. In this paper, the following cubic B-spline kernel function with C^2 continuity is used:

$$\Phi^a(\mathbf{x} - \mathbf{x}_I) = \begin{cases} \frac{2}{3} - 4\left(\frac{|\mathbf{x} - \mathbf{x}_I|}{a}\right)^2 + 4\left(\frac{|\mathbf{x} - \mathbf{x}_I|}{a}\right)^3 & \text{for } 0 \leq \frac{|\mathbf{x} - \mathbf{x}_I|}{a} \leq \frac{1}{2} \\ \frac{4}{3} - 4\left(\frac{|\mathbf{x} - \mathbf{x}_I|}{a}\right) + 4\left(\frac{|\mathbf{x} - \mathbf{x}_I|}{a}\right)^2 - \frac{4}{3}\left(\frac{|\mathbf{x} - \mathbf{x}_I|}{a}\right)^3 & \text{for } \frac{1}{2} \leq \frac{|\mathbf{x} - \mathbf{x}_I|}{a} \leq 1 \\ 0 & \text{otherwise} \end{cases} \quad (18)$$

Kernel functions with further higher order continuity may be used for evaluation of higher-order derivatives. The correction function is constructed to achieve reproducibility of polynomials in the approximation for convergence purposes or to reproduce specific functions representing important characteristics of the problem to be solved. In this work, we introduce monomial bases in the correction function for reproduction of n-th order monomials:

$$C(\mathbf{x}; \mathbf{x} - \mathbf{x}_I) = \sum_{|\alpha|=0}^n b_{\alpha_1 \alpha_2 \alpha_3}(\mathbf{x}) (x_1 - x_{1I})^{\alpha_1} (x_2 - x_{2I})^{\alpha_2} (x_3 - x_{3I})^{\alpha_3} \quad (19)$$

where

$$|\alpha| \equiv \sum_{i=1}^3 \alpha_i \quad (20)$$

Here, $b_{\alpha_1 \alpha_2 \alpha_3}(\mathbf{x})$ is determined so as to satisfy the following reproducing conditions for n-th order monomials,

$$\sum_{I=1}^{NP} \bar{\Phi}^a(\mathbf{x}; \mathbf{x} - \mathbf{x}_I) x_{1I}^{\alpha_1} x_{2I}^{\alpha_2} x_{3I}^{\alpha_3} = x_1^{\alpha_1} x_2^{\alpha_2} x_3^{\alpha_3}, \quad 0 \leq |\alpha| \leq n \quad (21)$$

Upon solving $b_{\alpha_1 \alpha_2 \alpha_3}(\mathbf{x})$ from Eq. (21) and substituting it back to Eqs. (19) and (17), we have the following RK approximation function:

$$\bar{\Phi}^a(\mathbf{x}) = \mathbf{H}^T(\mathbf{0}) \mathbf{M}^{-1}(\mathbf{x}) \mathbf{H}(\mathbf{x} - \mathbf{x}_I) \Phi^a(\mathbf{x} - \mathbf{x}_I) \quad (22)$$

where

$$\mathbf{H}^T(\mathbf{x} - \mathbf{x}_I) = [1, x_I - x_{1I}, \dots, x_3 - x_{3I}, (x_I - x_{1I})^2, \dots, (x_3 - x_{3I})^n] \quad (23)$$

$$\mathbf{M}(\mathbf{x}) = \sum_I \mathbf{H}(\mathbf{x} - \mathbf{x}_I) \mathbf{H}^T(\mathbf{x} - \mathbf{x}_I) \Phi^a(\mathbf{x} - \mathbf{x}_I) \quad (24)$$

6. Results and discussions

In the following model problem, the deformation of the grain structure is governed by the standard equilibrium equation, and the Galerkin weak form of equilibrium equation requires only C^0 -continuity in the test and trial functions. Thus finite element method is employed to obtain the displacement solution of the equilibrium equation of the grain structure. The identification of modulated patterns using incompatibility tensor, on the other hand, requires evaluation of second order derivatives of strain. It is noted that this evaluation of higher order derivatives using standard C^0 finite element approximation of displacement field requires averaging schemes that yields errors in the averaging processes. In this approach, we first use fine finite element discretization to model deformation of grain structure with refinement until the solution converges to desired accuracy. The finite element strains are then evaluated at the integration points and projected onto RK approximated strain field for evaluation of the incompatibility tensor and the corresponding strain gradient term for modulation identification.

Fig. 2 shows distribution of the plastic distortion along the cross section of the central grain as depicted by the solid line in Fig. 1(a). The FE plastic distortions evaluated at integration points are

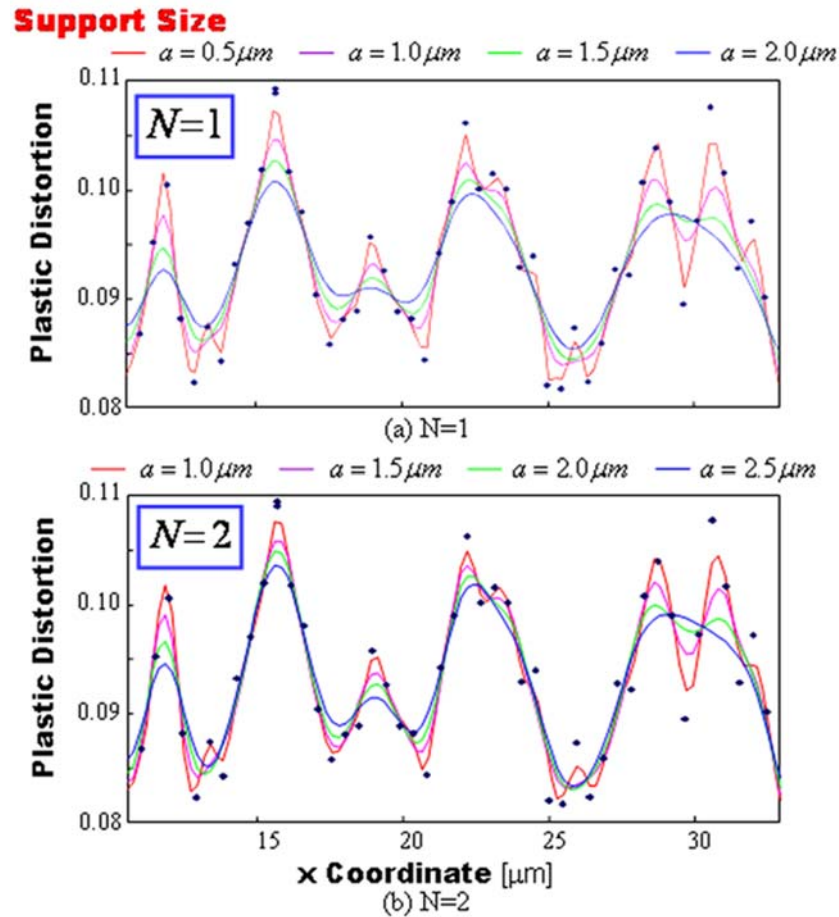


Fig. 2 Distributions of plastic distortion along transverse cross section of multi-grain model

indicated by dot symbols, and the plastic distortions obtained by the projection to the RK approximation are plotted by continuous lines. RK approximation with linear and quadratic monomial bases are denoted by $N=1$ and $N=2$, respectively, and solutions obtained by different support sizes “ a ” are compared in the figure. As can be seen, RK plastic distortion approximations with smaller support size better approaches finite element plastic distortion data at the integration points. This is expected as RK approximation functions are not interpolants in general, and using smaller support size in the RK approximation yields nearly interpolation properties. Increasing a , on the other hand, results in flatter distributions. In addition to the kernel function support size, the use of higher order monomial basis functions yields approximations closer to the data points.

The accuracy of the above FE solution has been confirmed via convergence study, where refinements of the finite element discretization are made until a convergence is reached. The displacement solution is obtained for coarser FE mesh models (those with 48×48 and 72×72 divisions) first in addition to the current model (with 96×96 divisions) and then examine the L2 norm of the solution difference between the consecutive mesh refinements. The L2 norm is defined here as the square root of the integral of the square of the solution difference over the whole

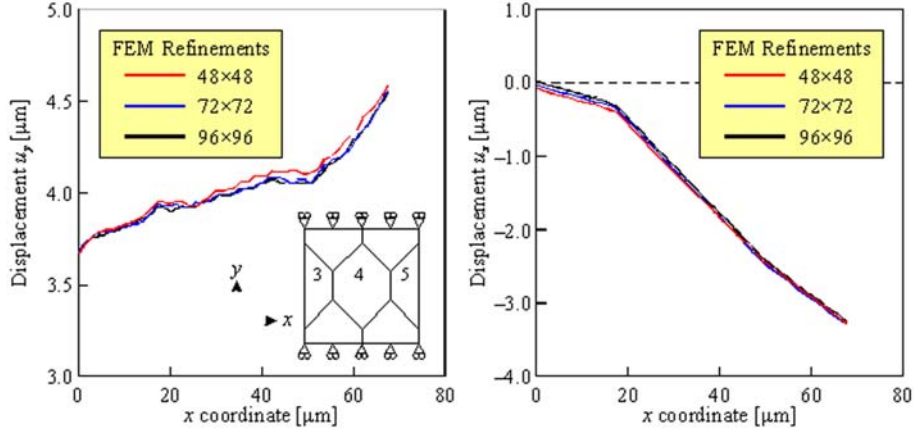


Fig. 3 Comparison of FE solutions for cross-sectional displacement of multi-grain model among three consecutive mesh refinements for convergence study

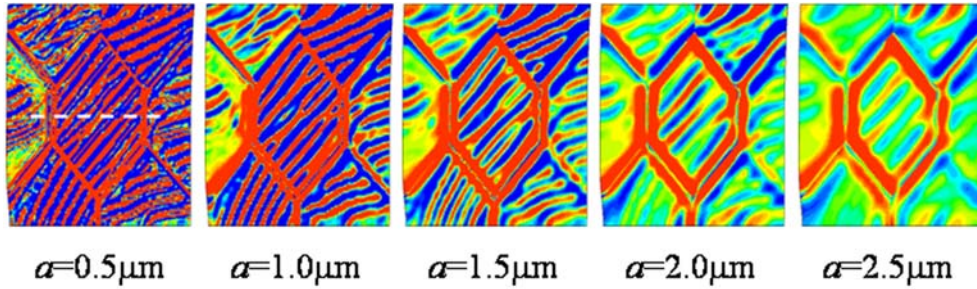


Fig. 4 Distributions of incompatibility term obtained by FEM

domain. The convergence criterion is set to be 1.0×10^{-4} . Fig. 3 compares the cross sectional distribution of the displacement solutions (for x and y directions) among the three models. The L2 norm between the adjacent two refinements u_y are 3.96×10^{-6} and 6.53×10^{-6} , respectively. Since they are much smaller than the convergence criterion, we can verify the sufficient accuracy of the current FE solution.

Fig. 4 shows distribution contours of the incompatibility term $F(\eta^{(1)})$ evaluated based on FEM utilizing a simple linear interpolation method for the plastic distortion field over the integration points of the elements within distance a as schematically shown in Fig. 5(a), and the derivatives of β_{ij}^p are then obtained by taking derivatives of finite element shape functions on the finite element interpolated β_{ij}^p . Here, the evaluation range a is varied from 0.5 to 2.5 μm , which has similar effects to the support size in RK approximation (Fig. 5).

As was discussed in the previous paper (Hasebe 2007), the use of the incompatibility tensor in the elasto-crystal plasticity-based simulations results in the emergence of modulated patterns as seen in, Fig. 4, which further yields modulations in stress, strain fields and the effective cell size distribution evaluated based on Eq. (10') (Hasebe 2007). One of the concerns here would be about the sensitivity of such modulated pattern formation to discretization resolution and the finite element evaluation method of the higher-order spatial derivatives. Fig. 4 also demonstrates that the evaluation range a essentially does not alter the modulation formation trend: Increasing range of the

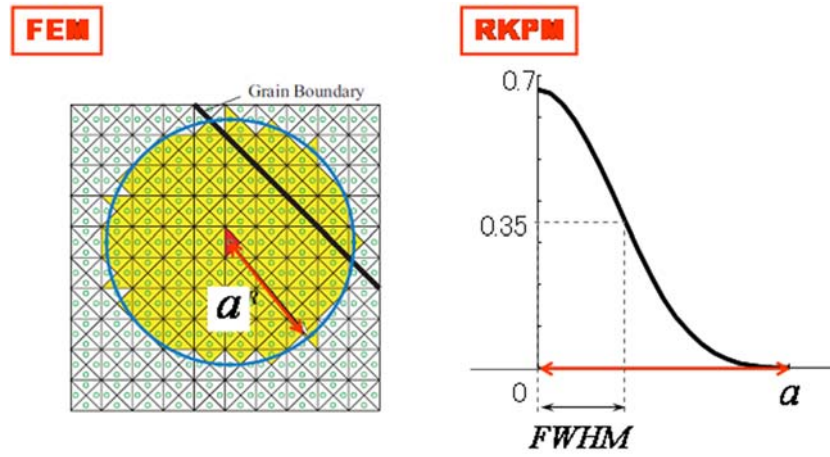


Fig. 5 Definition of range “ a ” for evaluation of derivative for (a) FEM and (b) RKPM

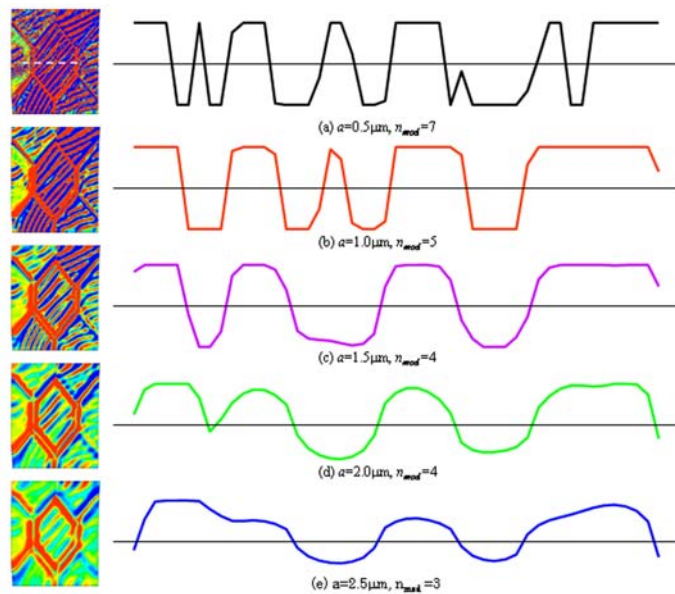
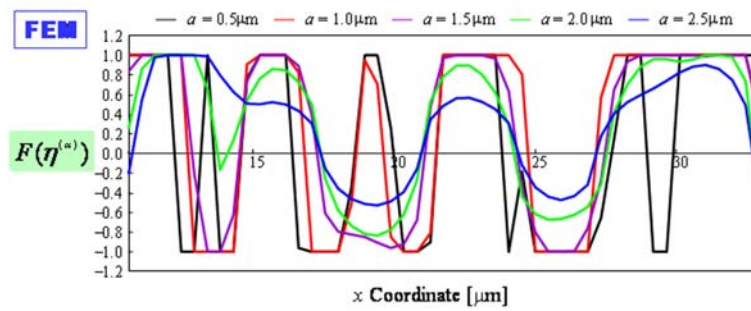


Fig. 6 Distributions of incompatibility term for central grain obtained by FEM

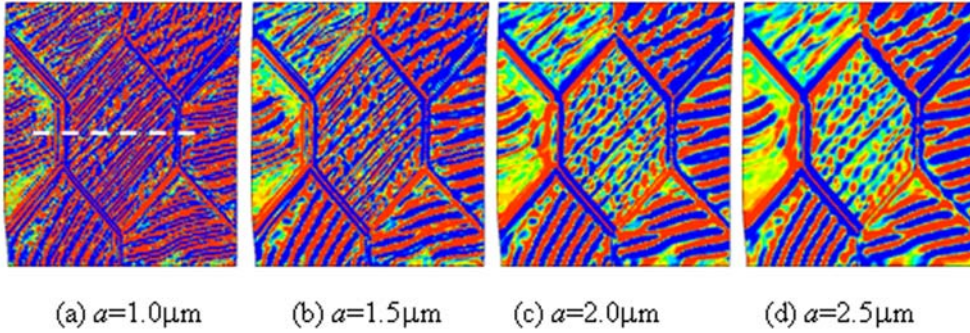


Fig. 7 Distributions of incompatibility term using RA approximation

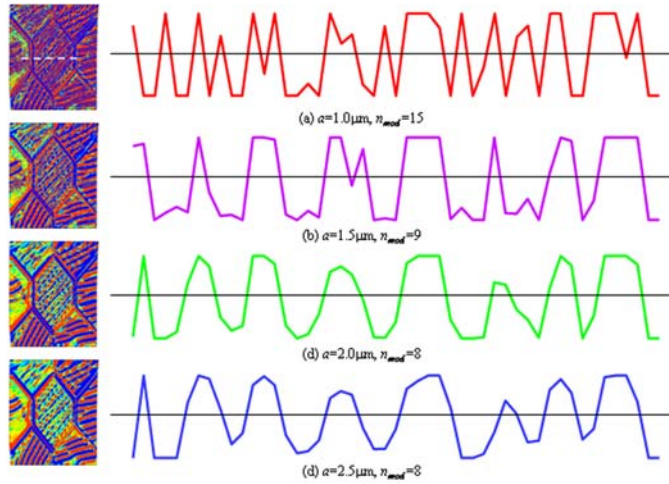
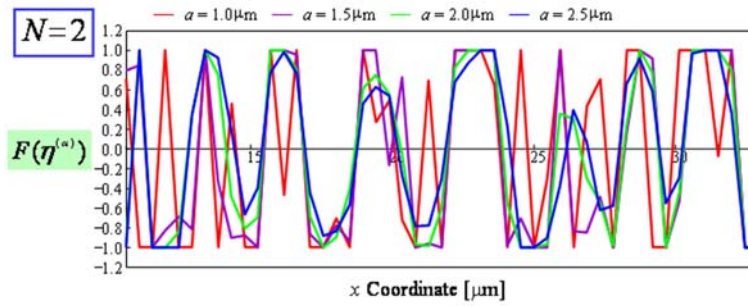


Fig. 8 Distributions of incompatibility term for central grain calculated by RK approximation ($N = 2$)

gradient evaluation simply tends to make the modulated patterns fuzzy due to a loss of local information. Note, the multiple levelset method will also be used for modeling such evolving microstructures as the above as in Zhang *et al.* (2008).

Fig. 6 compares the cross sectional distribution of the incompatibility term $F(\eta^{(1)})$ for the central grain obtained by FEM with different processing range a . A gradual transition from $a = 0.5$ to 2.5 without an abrupt change in the modulated distribution within this range. Note that a preliminary

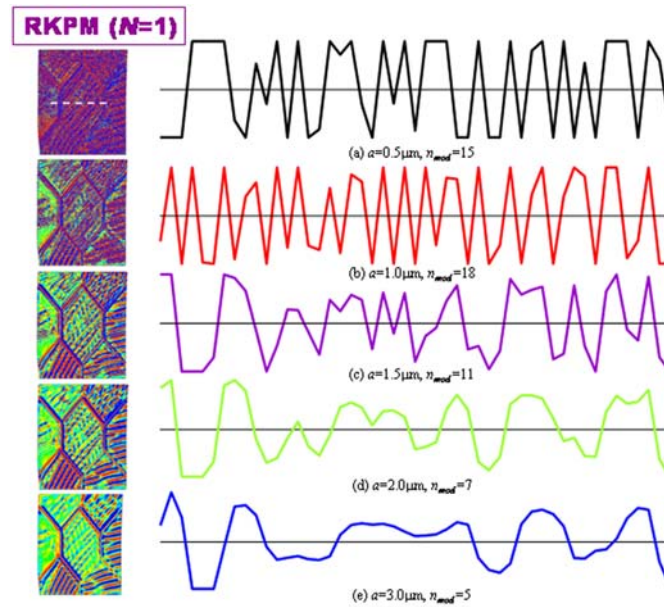


Fig. 9 Distributions of incompatibility term for central grain calculated by RK approximation ($N = 1$)

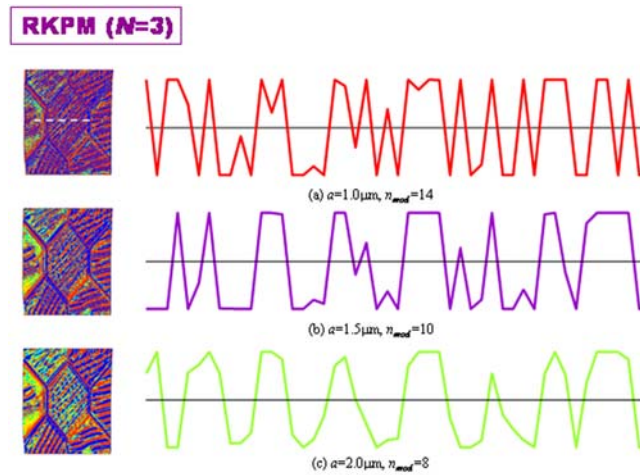


Fig. 10 Distributions of incompatibility term for central grain calculated by RK approximation ($N = 3$)

one-dimensional analysis over the wider range of a , i.e., up to around 20, showed that there exist such plateau-like regions periodically along with the increasing evaluation range, implying different physical meaning or picture systematically depending on the scales.

Fig. 7 show the incompatibility distribution obtained using the projected RK approximation, where monominal basis order $N = 2$ is employed. The support size is varied from $a = 1.0$ to 2.5 . The modulation patterns evaluated based on RK approximation are essentially similar to those by FEM, and exhibit smaller variation among different support size compared with the FEM-based results, except for $a = 1.0$. The result with the support size $3a = 1.0$ exhibits much finer modulation than the others, while the directions and morphology of the pattern are basically unaltered. Since this finer

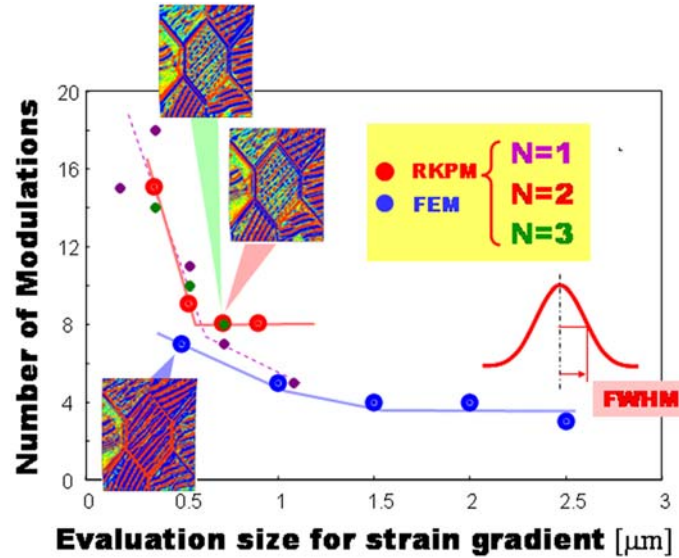


Fig. 11 Variation of modulations with a comparing FEM and RK-based evaluation of incompatibility terms.

modulation stem, at least partially, back to the non-smooth interpolation of the plastic distortion shown in Fig. 2, a careful examination would be further needed.

Figs. 8–10 display a comparison of the incompatibility distribution using different order of basis functions and different support sizes. Note that the minimum support size of the RK approximation is closely related to the order of basis functions used in the RK approximation so as to yield a non-singular moment matrix in Eq. (23); see Chen *et al.* for details. In general, the use of higher order bases in the RK approximation requires the employment of large kernel function support size for non-singular moment matrix. Similarly to the trend observed in finite element calculation shown in Fig. 6, a gradual transition of the modulation from $a = 1.5$ to 2.5 is observed, and the cases for $a = 2.0$ and 2.5 yield almost identical results.

For a quantitative comparison, the number of modulations observed in the central grain is counted in Figs. 8–10 and is summarized in Fig. 11. As a possible interpretation, the full width at half maximum (FWHM, see Fig. 5(b) for the definition) of the kernel function with support size a is employed here for the comparison with the FEM-based results. The RK-processed results exhibit larger modulation numbers than those of FEM, essentially due to the higher order continuity in the approximation, and shows a fast convergent when support size is greater than $a = 1.5$. The FEM-based results, on the other hand, shows a much slower convergence.

It is imperative to point out that the morphological features as well as the number of the modulated patterns based on the incompatibility tensor are essentially unaffected by the material parameters used in the incompatibility term, i.e., l_{defect} and p_η in Eq. (12). They control the intensity of the incompatibility term and ultimately affect the effective cell size d_{cell} (Eq.(10')) to be evaluated from the hardening ratio $Q_{\alpha\beta}$. In this sense, the present model is insensitive to l_{defect} and p_η as far as the morphology of the modulation is concerned. Note, an introduction of the interactions with smaller scale inhomogeneities than the grain size, e.g., that measured by d_{cell} , may change both the modulation number and the morphology, which is one of the future scopes of the present study. The interaction effects will be separately discussed in the other papers (Hasebe 2009a, 2009b).

7. Conclusions

The present study demonstrates that basic morphology of the modulated patterns including the directionality can be obtained by computing the incompatibility tensor. The crystallography reflects the slip system and associated slip deformations that are closely related to the crystal orientation and the imposed deformation mode. The experimentally-observed dislocation substructures in terms of the morphology have also been shown in some specific cases (Sugiyama 2005).

The number of modulations, on the other hand, is shown to be affected by the evaluation method for strain gradients in the incompatibility and distortion tensors as demonstrated above. Particularly, we have shown that the number of modulations in the incompatibility tensor distribution is affected by the support size of the RK approximation or the “processing zone” of strain derivative averaging in the FEM approximation. We further showed that the number of modulations converges faster as the support size increases in the RK approximation compared to the case based on the FEM. This implies a significant possibility in applying RK approximation to express multiple inhomogeneous fields under different physical conditions in different scale levels by evaluating the incompatibility tensor with properly selected kernel smoothness (order of continuity), support size, and basis functions in the RK approximation.

The proposed RK approximation offers a straightforward and accurate calculation of higher order derivatives of strain involved in the incompatibility tensor compared to that based on finite element interpolation and averaging procedures. This approach becomes even more critical for simulation of finer scale evolving dislocation substructures based on incompatibility or distortion tensors.

References

- Aoyagi, Y. and Hasebe, T. (2007), “New physical interpretation of incompatibility and application to dislocation substructure evolution”, *Key Engineering Materials*, **340-341**, 217-222.
- Chen, J. S., Pan, C., Wu, C. T. and Liu, W. K. (1996), “Reproducing kernel particle methods for large deformation analysis of nonlinear structures”, *Comput. Methods Appl. Mech. Eng.*, **139**, 195-227.
- Hasebe, T. (2004a), “Continuum description of inhomogeneously deforming polycrystalline aggregate based on field theory”, *Mesosopic Dynamics of Fracture Process and Materials Strength, IUTAM Symp.* (eds. Kitagawa, H., Shibutani, Y.), 381-390, Kluwer.
- Hasebe, T. (2004b), “Field theoretical multiscale polycrystal plasticity”, *Trans. MRS-J*, **29**, 3619-3624.
- Hasebe, T. (2006), “Multiscale crystal plasticity modeling based on field theory”, *CMES*, **11-3**, 145-155.
- Hasebe, T. (2009a), “Field theory-based description of interaction field for multiple scales: Part I-theory-”, *Interaction and Multiscale Mechanics, An Int. J.*, **2**(1).
- Hasebe, T. (2009b), “Field theory-based description of interaction field for multiple scales: Part II-Application-”, *Interaction and Multiscale Mechanics, An Int. J.*, **2**(1).
- Liu, W. K., Jun, S. and Zhang, Y. F. (1995), “Reproducing kernel particle methods”, *I. J. Numer. Methods Fluids*, **20**, 1081-1106.
- Sugiyama, M. (2005), Private communication.
- Wang, D. and Wu, Y. (2008), “An efficient Galerkin meshfree analysis of shear deformable cylindrical panels”, *Interaction and Multiscale Mechanics, An Int. J.*, **1**(3), 339-355.
- Zhang, X., Chen, J. S. and Osher, S. (2008), “A multiple level set method for modeling grain boundary evolution of polycrystalline materials”, *Interaction and Multiscale Mechanics, An Int. J.*, **1**(2), 191-209.